Research article **Open Access**

Xiaoshuai Liu, Jianbin Huang, Yuchao Li, Yao Zhang* and Baojun Li*

Rotation and deformation of human red blood cells with light from tapered fiber probes

DOI 10.1515/nanoph-2016-0115
Received April 5, 2016; revised June 2, 2016; accepted June 29, 2016

Abstract: Dynamic rotation and deformation of human red blood cells (RBCs) are extremely important to investigate the survival and mechanical features of cells, which will be of great physiological and pathological significance. Here, we report an optical approach that is capable of both rotating and deforming RBCs with light from two tapered fiber probes (TFPs). With laser beams at the wavelength of 980 nm injected into the TFPs, a single RBC was rotated around different axes while single or multiple RBCs were stretched by adjusting the points of action and magnitude of the optical forces from the TFPs. The biological safety of the approach was also discussed by taking the laser power required into account.

Keywords: biophotonics; optical tweezer; cell manipulation; cell analysis.

1 Introduction

Red blood cells (RBCs) play an important role in cell metabolism and aerobic respiration [1, 2]. The physical and mechanical features of RBCs have been regarded as an important indicator in the studies of bio-processes, pathology, and toxicology [3, 4]. Flexible and precise manipulation of RBCs, especially controllable rotation and deformation, promises more understandings of cell structure at the nanoscale and offers new insights into the vascular disease diagnoses [5–7], tomographic microscopy [8], cell microrotor [9], mechanotransduction and chemical release [10–12]. To date, methods to rotate RBCs have been proposed based on the dielectrophoretic [13], dual-beam spanner [14], and confocal fluorescence microscopy [15], while the deformation of RBCs has also been demonstrated with microfiltration [16], diffraction ektacytometry [17], micropipette aspiration [18], electric field [19], and atomic force microscopy [20]. However, the function of these devices or platforms was limited to either rotation or deformation. To achieve diverse investigation of physical and mechanical features of RBCs in a simple and efficient way, a combination of the functions of both rotation and deformation within a single device or platform is highly expected. As a candidate for manipulating microparticles and cells [21], tapered fiber probes (TFPs) have advantages of small size and ease in fabrication, which has been demonstrated to arrange cells in a chain and further to perform the precise regulation of cell chain [22]. Here, we demonstrate the rotation and deformation of RBCs with light from TFPs. By adjusting the points of action and magnitude of the optical forces from the TFPs, a single RBC can be rotated around different axes of the cell. Besides, single or multiple RBCs can be stretched, providing the potential application to investigate the interaction between deformed cells.

2 Results and discussion

Figure 1A shows the scheme of RBC rotation around the optical axis of TFP (defined as *x* axis in Figure 1A). Two fiber probes, i.e. TFPs 1 and 2 shown in Figure 1A, were fabricated with flame-heating technique (see Methods for the fabrication). The structure details of the probes are shown in Figure S1 in the Supplementary Materials. One side of RBC was bound to TFP 1 tip by the optical forces (generated by TFP 1) and Van der Waals force. The wavelength of laser beam was set at 980 nm due to the low absorption for the biological cells [23]. Such a wavelength induces little optical damage to bacteria and mammalian cells [24]. After injecting the 980-nm laser beam

***Corresponding authors: Yao Zhang and Baojun Li,** State Key Laboratory of Optoelectronic Materials and Technologies, School of Materials Science and Engineering, Sun Yat-Sen University, Guangzhou 510275, China, e-mail: zhyao5@mail.sysu.edu.cn (Y. Zhang); stslbj@mail.sysu.edu.cn (B. Li)
Xiaoshuai Liu, Jianbin Huang and Yuchao Li: State Key Laboratory of Optoelectronic Materials and Technologies, School of Materials Science and Engineering, Sun Yat-Sen University, Guangzhou 510275, China

©2016, Yao Zhang, Baojun Li et al., published by De Gruyter.
This work is licensed under the Creative Commons Attribution-NonCommercial-NoDerivatives 3.0 License.

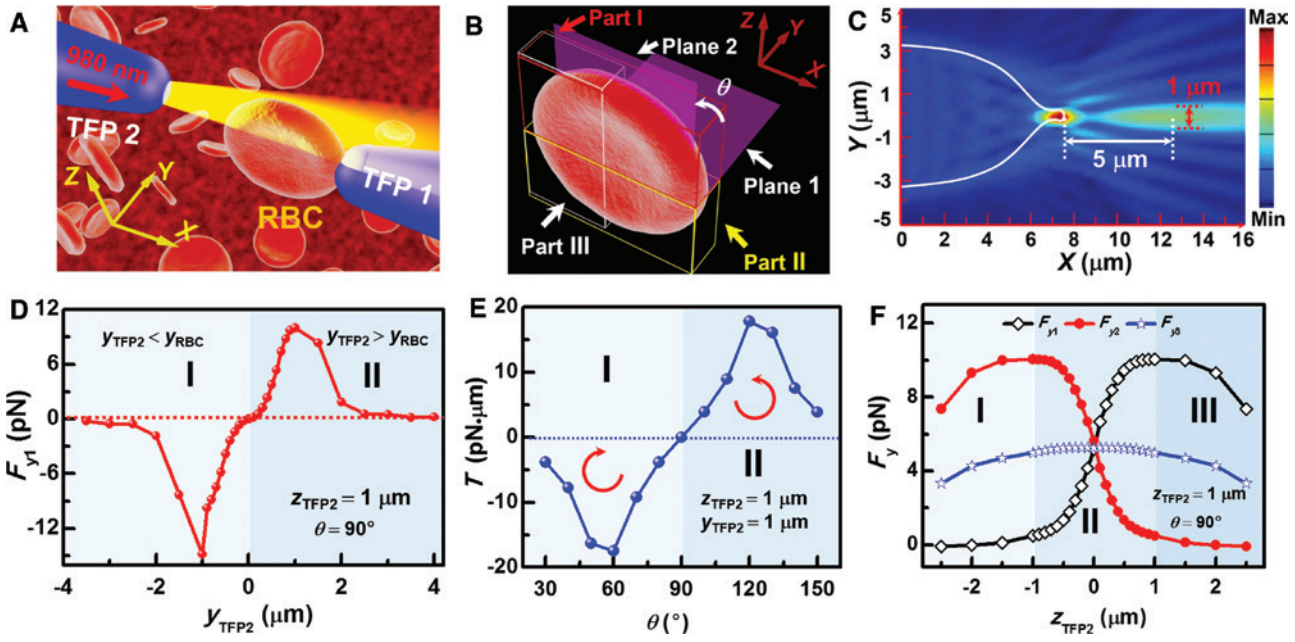

Figure 1: (A) Schematic of RBC rotation around the *x* axis. (B) Schematic of the RBC profile. (C) Simulated *E*-field distribution of light from TFP 2 tip. (D) Optical force F_{y1} as a function of y_{TFP2} (z_{TFP2}=1 μm and θ=90°). (E) Optical torque *T* as a function of θ (y_{TFP2}=0 μm and z_{TFP2}=1 μm). Red arrows indicate the cell rotation direction. (F) Optical forces F_{y1}, F_{y2}, and F_{y3} exerted on part I, II, and III of cell as a function of z_{TFP2} (y_{TFP2}=1 μm and θ=90°).

into TFP 2, the upper part of RBC can be trapped and then shifted along the *y* direction by adjusting TFP 2. Due to the binding of a part to TFP 1 tip, the RBC will suffer from an optical force torque, under which the cell will be rotated around the *x* axis. As shown in Figure 1B, the red, yellow, and white wireframes indicate the upper (Part I), lower (Part II), and left (Part III) parts of the RBC, respectively. The *x*-*y* plane and orientation plane of the cell were defined as planes 1 and 2, respectively. The orientation angle (θ) of the cell was between planes 1 and 2 so that θ was 90° before the laser beam was injected into TFP 2. To numerically analyze the rotation process, the electric field (*E*-field) distribution of the beam from TFP 2 tip was obtained by a three-dimensional (3D) finite difference time domain simulation (see Section 2 in the Supplementary Materials for the calculation details). Figure 1C shows the *E*-field distribution in the *x*-*y* plane. The laser power (P_2) injected into TFP 2 was set as 24 mW, which is consistent with the following experiment. The focal plane (with the strongest light intensity) of the output laser beam is 5 μm away from the probe tip. At the focal plane, over 90% of the *E*-field intensity distributes within the region from *y*=-0.5 to 0.5 μm. Thus, when an RBC (average diameter: 6.2 μm) was located at the focal plane, a specific part (I, II, or III) rather than the whole cell can be trapped. For example, at $z_{TFP2}>z_{RBC}$, the focal plane was near the upper part of the cell so that part I can be trapped.

Optical forces exerted on the cell were then calculated by taking the integral of Maxwell stress tensor obtained from the simulations. Figure 1D shows the optical force exerted on part I in the *y* direction (F_{y1}) as a function of y_{TFP2} (at z_{TFP2}=1 μm and θ=90°). F_{y1} was defined as negative and positive for the forces along the -*y* and +*y* directions, respectively. At $y_{TFP2}<y_{RBC}$ (region I) and $y_{TFP2}>y_{RBC}$ (region II), F_{y1} was negative and positive, respectively. Thus, part I will move toward TFP 2 in the *y* direction. Then the RBC will suffer from the optical force torque (*T*), under which the cell will be rotated around the *x* axis. Figure 1E shows the calculated optical torque at different orientation angles. With TFP 2 fixed at y_{TFP2}=0 μm and z_{TFP2}=1 μm, the cell suffers from the negative and positive torque at 30°<θ<90° (region I) and 90°<θ<150° (region II), respectively. Thus, the cell will be rotated around *x* axis clockwise and anticlockwise from the view of light propagation direction, respectively. Finally, the cell will be orientated at θ=90° due to *T*=0. When TFP 2 was shifted along the *y* direction, the cell can be orientated at different angle so that it will be continuously rotated around *x* axis.

The trapped part can be changed by adjusting TFP 2 along the *z* direction and further realizing the rotation around different axes. Figure 1F shows F_y exerted on part I (F_{y1}), part II (F_{y2}), and part III (F_{y3}) as a function of z_{TFP2} (y_{TFP2}=1 μm and θ=90°). When TFP 2 was above the cell center in the *z* direction (i.e. 0.5<z_{TFP2}<3 μm, region III), F_{y1}

was larger than F_{y2} so that part I of the cell will be trapped and then moved with TFP 2. When TFP 2 was below the cell center (i.e. $-3<z_{TFP2}<-0.5$ μm, region I), F_{y1} was smaller than F_{y2} so that part II will be trapped by TFP 2 and the cell will be rotated clockwise with TFP 2 shifted along the $+y$ direction. In region II ($-0.5<z_{TFP2}<0.5$ μm), part I and II of the cell will suffer from nearly the equivalent optical forces, which leads to a counteraction of the torque around the x direction. Meanwhile, since F_{y3} is positive, part III of the cell will move toward the $+y$ direction so that the cell will be rotated around the z axis rather than the x axis with TFP 2 shifted along the y direction. Note that in the presented approach, the cell rotation was mainly affected by the magnitude of the optical trapping force exerted on the cell. Since the optical trapping force was only related to the cell refractive index, laser wavelength, and the local optical gradient, other physical properties (e.g. chirality) of the cells have very little effect on the rotation. To trap a specific part, the cell is required to have a low absorption to the laser beam. Otherwise, the cell will be pushed away rather than trapped by the probe and cannot be controllably rotated. Moreover, the high absorption will induce considerable damages to cells, which decreases cell bioactivity. Further, single or multiple RBCs can be stretched by the optical force generated by the laser beams from two TFPs, which will also be demonstrated in the following sections.

Before rotation, one side of the RBC was bound to the TFP 1 by the optical force and Van der Waals force (see Methods for RBC sample preparation and the binding process). Schematic and detailed descriptions of the experimental setup are in section 3 in the Supplementary Materials. The experiments were started by launching the 980-nm-wavelength laser beam into TFP 2 at P_2=24 mW. At t=0 s, one RBC was bound to the tip of TFP 1 at θ=0° (Figure 2a1). With TFP 2 shifted along the $-y$ direction, the cell was rotated around the x axis and θ gradually increased (Figure 2a2–5). At t=10 s (Figure 2a6), by shifting TFP 2 along the $+y$ direction, θ decreased and finally remained at θ=0° (Figure 2a7–10). The detailed rotation process is demonstrated by Movie S1 in the Supplementary Materials. y_{TFP2} and θ in this rotation process were obtained (Figure 2B). From t=0 to 3.8 s (region I), TFP 2 was shifted along the $-y$ direction with a distance of 3.3 μm, and θ increased from 0° to 90°. Then θ remained 90° from 3.8 to 5 s (region II), indicating that an orientation of the cell at a certain angle can also be realized by manipulating TFP 2. At t=5 s, with TFP 2 shifted along the $-y$ direction again, θ increased from 90° to 172° (region III). Then θ remained 172° from t=7 to 9.5 s with TFP 2 kept stationary (region VI). The results confirm that cell can be stopped at a certain angle. To show the stability of cell orientation, the deviation of cell orientation angle around 172° ($\Delta\theta$) was estimated, as shown in Figure S4 in the Supplementary Materials.

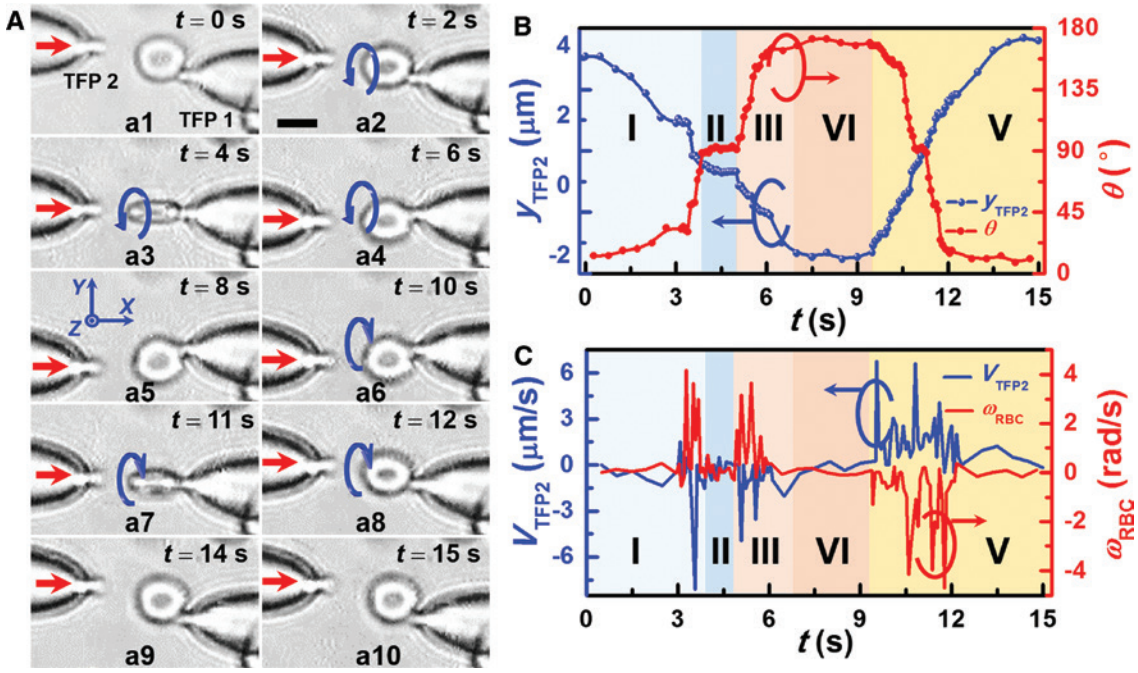

Figure 2: RBC rotation around the x axis. (A) Optical microscopic images for rotating an RBC around the x axis. Scale bar: 5 μm. (B) Calculated y_{TFP2} and θ in the rotation process. (C) Calculated V_{TFP2} and ω_{RBC} in the rotation process.

After that, TFP 2 was shifted along the -y direction from t=9.5 to 15 s so that θ decreased from 172° to 0° (region V). Thus, a controllable rotation and orientation of the RBC around the x axis can be realized by manipulating TFP 2. The shifting velocity of TFP 2 (V_{TFP2}) and angular velocity of RBC (ω_{RBC}) were also calculated (Figure 2C). The value of ω_{RBC} monotonously varied with V_{TFP2}, with a maximum of 4.7 rad/s. However, it should be noted that ω_{RBC} was not liner with V_{TFP2} so that obtaining a constant ω_{RBC} required a variant V_{TFP2}, which can be realized by precisely manipulating the six-axis microstages (resolution 50 nm). Further, the accuracy of RBC rotation velocity (ε_{cell}) was calculated from the experiment, which can be defined as

$$\varepsilon_{cell} = |\Delta\omega|_{max}/\omega_0, \quad (1)$$

where ω_0 and $|\Delta\omega|_{max}$ indicate the cell average rotation velocity and the maximum value of velocity deviation, respectively. The results show that ε_{cell}=±1.5–3%, which also depended on the magnitude of ω_{RBC}. The accuracy of ε_{cell} can be further optimized with the assistance of a programmable stepper motor. Note that at θ=0°, if TFP 2 was shifted along the +y rather than the -y direction, the RBC will be rotated around the z axis (see Figure S5 in Supplementary Materials).

As indicated by the results of the optical forces shown in Figure 1F, at θ=90°, if TFP 2 was shifted along the z direction to coincide its optical axis with the cell center in the z direction (i.e. z_{TFP2}=z_{RBC}=0 μm), part III of the cell will be trapped by TFP 2. Therefore, when TFP 2 was shifted along the y direction, the cell will be rotated around the z axis, as schematically shown in Figure 3A. The experiment was also conducted by injecting the laser beam into TFP 2 at P_2=24 mW. At t=0 s, TFP 2 was adjusted along the z direction to trap part III of the cell (Figure 3b1). With TFP 2 shifted along the -y direction, the cell was gradually rotated anticlockwise with an angle (θ_2) of 90° (Figure 3b2–5). With TFP 2 shifted along the -y direction again, the cell escaped from the optical trap and was orientated along the optical axis of TFP 1 (Figure 3b6–9). y_{TFP2} and θ_2 in this process were also obtained (Figure 3C). In region I (from t=0 to 0.3 s), θ_2 increased from 0° to 45°, with TFP 2 shifted along the -y direction with a distance of 3 μm. By remaining TFP 2 stationary for 0.2 s (region II), the cell was orientated at θ_2=45°. The deviation of cell orientation angle around 45° ($\Delta\theta$) was also estimated, as shown in Figure S4 in the Supplementary Materials. With TFP 2 shifted along the -y direction again with a distance of 4 μm (region III), θ_2 increased from 45° to 90°. With TFP 2 further shifted along the -y direction, the cell was gradually rotated clockwise so that θ_2 decreased from 90° to 0° (region VI), indicating that the cell escaped from the optical trap. Note that diverse rotations of the RBC, including the rotation around the x and z axes simultaneously, can also be realized by precisely manipulating TFP 2 (see Figure S6 in the Supplementary Materials). Moreover, in a droplet of RBC solution on a glass slide, some RBCs will descend to the bottom and be attached to the slide surface via Van der Waals forces. In this case, the RBCs can be rotated with only one TFP (see Figure S7 in the Supplementary Materials).

As mentioned in previous sections, by using the two TFPs, a stretch of single or multiple RBCs can also be

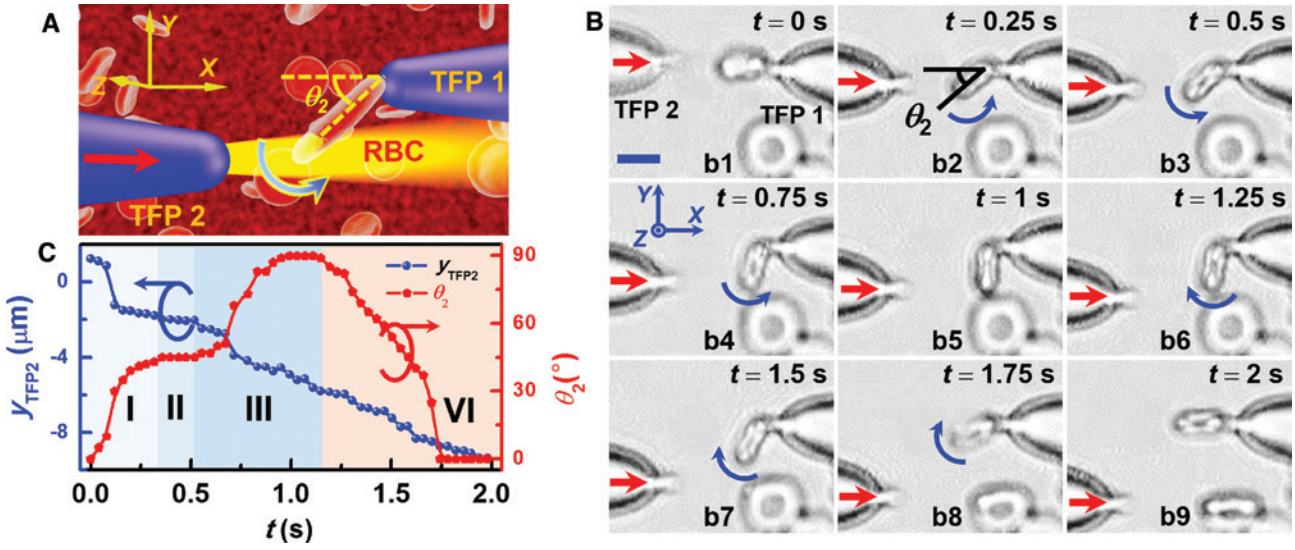

Figure 3: RBC rotation around the z axis. (A) Schematic of RBC rotation around the z axis. (B) Optical microscopic images for rotating an RBC around the z axis. Scale bar: 5 μm. (C) Calculated y_{TFP2} and θ_2 in the rotation process.

realized. For illustration, a simultaneous stretch of multiple RBCs is demonstrated here. As schematically shown in Figure 4A, after injecting the laser beams into both TFPs 1 and 2, three RBCs are trapped and then stretched along the optical axis of TFPs. With the same experimental setup as that for RBC rotation, two and three RBCs were stretched simultaneously, as shown in Figure 4B and C, respectively. Before turning on the lasers, two RBCs, with diameters of 5.6 and 6.4 μm, were located between the two TFPs (Figure 4b1). The gap between the two RBCs was 2 μm. Then, two 980-nm-wavelength laser beams were injected into the two TFPs and the power into TFPs 1 (P_1) and 2 (P_2) was P_1=P_2=20 mW. After turning on the laser for 6 s, the RBCs moved toward each other until they became contacted due to the optical force (Figure 4b2). Meanwhile, they were gradually stretched until they reached equilibrium at t=10 s (Figure 4b3). The degree of deformation of the RBCs can be described by the shear strain (γ), which was defined as $\gamma=\Delta l/l$, where Δl and l are lengths of the cell before and after stretching, respectively. At t=10 s (Figure 4b3), the shear strains of the two cells were 0.14 and 0.12, and the cells were kept stretched until the laser was turned off at t=35 s (Figure 4b4). After that, the RBCs gradually resumed their original shapes (Figure 4b5, 6). The detailed deformation process is demonstrated by Movie S2 in the Supplementary Materials. Similarly, a simultaneous stretch of three RBCs was also conducted, as shown in Figure 4C. The diameters of RBCs 1, 2, and 3 were 6.7, 5.7, and 6.9 μm, respectively (Figure 4c1). After turning on the laser, the RBCs began to be trapped and then stretched (Figure 4c2).

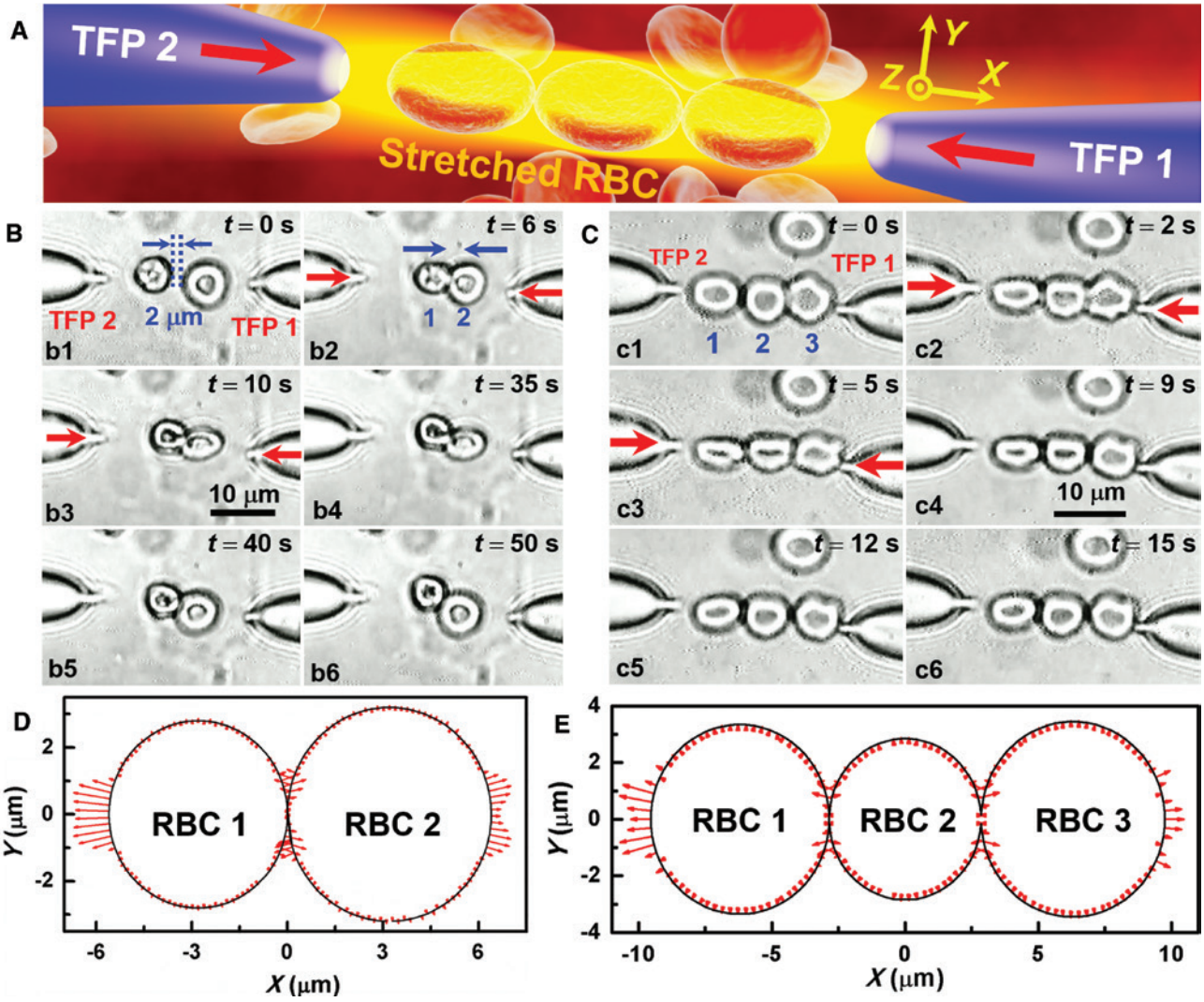

Figure 4: Stretching multiple RBCs with light from two TFPs. (A) Schematic of stretching multiple RBCs by using two TFPs. (B) Optical microscopic images for stretching two RBCs. (C) Optical microscopic images for stretching three RBCs. (D) Stress distribution on the surfaces of the two RBCs. (E) Stress distribution on the surfaces of the three RBCs.

The distance between the cells decreased with the increase in γ, and the cells gradually became contacted with each other. At t=5 s, the three cells reached equilibrium with γ=0.15, 0.1, and 0.12 (Figure 4c3). By turning off the laser at t=9 s, RBCs started to resume their original shapes (Figure 4c4–6). Normalized stress distribution on the surfaces of the RBCs was also investigated, as indicated by the red arrows in Figure 4E and F. The stress was mainly distributed along the x axis and the direction of the stress was toward the outside of cells. Therefore, the RBCs were stretched and further became contacted with each other. In addition, due to the different cell sizes and distances to the TFPs, the average stress exerted on the RBCs was also different so that the stretched RBCs had different values of γ, which was consistent with the experimental observation that the degrees of deformation of the RBCs were also different. Note that a single cell can also be stretched with this technique (see Figure S8 in the Supplementary Materials). Moreover, for the RBCs with one side attached to the slide surface via Van der Waals forces at the bottom of a droplet, the cells can also be stretched with only one TFP (see Figure S9 in the Supplementary Materials).

The biological safety of the presented method should also be of concern since it is developed for biological applications. Although the laser wavelength with a low absorption was applied to perform the cell rotation and deformation, a proper level of the laser power is also required to avoid potential radiation damage to the RBCs. The viability of the cells can be characterized by adding 5% (volume) Trypan Blue to the cell solution [25]. Living cells can prevent the dye from penetrating the cytoplasm while the dead cells cannot so that the dead cells will appear blue. To choose a proper level of laser power, the rotation and deformation of RBCs were performed with different laser powers, and the Trypan Blue was added into the solution after rotation or deformation in each test. Ten minutes after adding the dye into the solution, the results showed that for RBC rotation, no RBC could be trapped and rotated at P_2<10 mW; at $10 \le P_2 \le 60$ mW, the specific parts of the RBCs were trapped and then rotated, and no staining on the cells was observed, which indicates that the cells survived in the rotation process; at P_2>60 mW, the RBCs were gradually stained to blue, indicating that the cells suffered from the phototoxicity and cannot maintain their normal functions. For RBC deformation, no RBCs were trapped and stretched at $P_1=P_2$<8 mW; at $8 \le P_1=P_2 \le 40$ mW, the RBCs were trapped and then stretched, and no staining on the cells was observed, which indicates that the cells survived in the stretching process; at $P_1=P_2$>40 mW, the RBCs were gradually stained to blue, indicating that the cells were over the elastic deformation and even ruptured. Therefore, to ensure that the RBCs were deformed without any irreversible damages, P_1 and P_2 should range from 8 to 40 mW. Note that the proper power range also varies with the distances between the two TFPs due to further divergence of the laser beams from the TFPs.

Note that in principle, human cells larger than RBCs can also be rotated with the presented technique. However, it becomes more challenging to rotate the larger cells because they suffer from more fluid resistance during the rotation process, leading to a higher laser power of TFP 2 (P_2) required to reach the same rotation velocity as RBCs. In addition, as presented in the experimental results above, the cell was under rotation at a relatively low velocity (ω_{RBC}<6.5 rad/s) so that the cell contents suffered little impact and the normal functions of the cells could remain during the rotation. It should also be pointed out that in some applications, such as tomographic imaging, deformation of the cells should be avoided during cell rotation. In our experiments of cell rotation, there were no observable deformations on the cells; i.e. the cells were only under a controllable rotation around different axes. However, when the cell reached its maximum orientation angle (e.g. θ=172° in Figure 2a5), it could be stretched with TFP 2 further shifted along the -y direction, which was similar to the case shown in Figure S9. Note that for the cell deformation with only one TFP, the required laser power (P_2) to stretch cells was higher than 45 mW; otherwise, the cell will escape from the optical trap of TFP 2, as shown in Figure 3b6–9. Therefore, the deformation can be avoided by rotating the cell within a range of orientation angles smaller than the maximum and with a low laser power (P_2<45 mW) during the rotation.

Recent studies have demonstrated the remarkable ability to realize the controllable rotation of optically trapped RBCs using holographic optical tweezers (HOTs) [8, 26] and conventional optical tweezers (COTs) based on non-rotationally symmetric trapping beams [27] or circularly polarized light [9]. However, for the COT and HOT approaches, once the optical traps were set, the cells can only be rotated around a predesigned axis. Compared to the COT and HOT approaches, the presented method of trapping and rotating RBCs using one or two TFPs is able to achieve rotations around several different axes by simply manipulating the TFPs. Besides, by using the TFPs, the cell rotation is free from the operation depth limit, which still exists in the COT or HOT systems due to the short working distance of a high numerical-aperture objective. Further, TFPs, with the features of ease in fabrication and very small sizes, provide a much more compact configuration than do the bulky optical systems consisting of a series of objectives. Recent studies have also demonstrated that the RBCs can be stretched using two cleaved

optical fiber, which is called an optical stretcher [25, 28]. Compared to the optical stretcher, the parabolic shape of the TFP tips provides a stronger focusing effect for outputted laser beams. To obtain the same shear strain, the laser power required for stretching the cells was decreased from hundreds of milliwatts (required for the COT or HOT approaches) to tens of milliwatts. In addition, by using the TFPs, multiple RBCs can be stretched simultaneously, which has not been demonstrated by using an optical stretcher.

3 Conclusions

Optical rotation and deformation of human RBCs were demonstrated by using two TFPs. After one side of the cell was bound to the tip of TFP 1, the cell was rotated around different axes by manipulating the TFPs. Single or multiple RBCs can be stretched simultaneously with light from two TFPs. The presented method provides a perspective to dynamically manipulate the cell for investigating the physiological roles of RBCs, which is anticipated to be useful in the diagnosis and treatment of blood vascular diseases.

4 Methods

4.1 Fabrication of the fiber probe

In the experiment, two specially designed tapered optical fibers were used, which were fabricated using the commercial single-mode optical fibers (connector type: FC/PC, core diameter: 9 μm, cladding diameter: 125 μm; Corning Inc.) with a flame-heating technique. First, the buffer and polymer jacket of fibers were stripped off with a fiber stripper, and then the fibers were sheathed with a glass capillary (inner diameter: ~0.9 mm, wall thickness: ~0.1 mm, length: ~120 mm) to protect them from breakage and warping. Second, after being heated for approximately 1 min to reach their melting point, the heated fibers were drawn with an initial speed of about 0.5 mm/s. Meanwhile, the fiber diameters were decreased from 125 μm to 7.8 μm over a 2-mm length, which is a gradual taper shape. It was followed by an abruptly tapered region in which the diameter decreased from 7.8 to 0.5 μm over a distance of 6 μm. Finally, the fibers were broken with the drawing speed increased to be about 2 mm/s. Then, the TFPs were fabricated with specific abrupt tapered tips at the end. The structure details of the probes are shown in Figure S1 in the Supplementary Materials.

4.2 Preparation of the RBC sample

The sample was obtained by drawing ~20 μl blood at the fingertip from a healthy adult male and then collected in a sterile anticoagulant containing glucose and sodium citrate. After being centrifuged at 2500 rpm for 10 min, the plasma and white blood cells were aspirated out. Then the purified RBCs were diluted in a phosphate buffer solution with a cell concentration of about 3×10^4 #/ml.

4.3 Binding one side of the RBC to the TFP 1 tip

After the RBC solution was dropped onto the glass slide, TFP 1 was dipped into the solution to approach a specific RBC by manipulating the microstage that held the fiber. With a 980-nm laser beam injected into TFP 1 with a power of 30 mW, the cell was trapped onto the probe tip by the optical gradient force. After turning off the laser, one side of the cell was bound to the probe tip via Van der Waals force.

5 Supplementary materials

Further details are enclosed as supplementary materials, including the numerical simulations, diversified rotation of cells, evaluation of the stability of cell orientation, single cell deformation with only one or two TFPs, and two video clips (Movies S1 and S2) to present the detailed processes of the RBC rotation around *x* axis and the deformation of two cells. This material is available to authorized users.

Acknowledgments: This work was supported by the Program for Changjiang Scholars and Innovative Research Team in University (IRT13042), the National Natural Science Foundation of China (no. 61205165).

References

[1] Wan JD, Forsyth AM, Stone HA. Red blood cell dynamics: from cell deformation to ATP release. Integr Biol 2011;3:972–81.
[2] Tomaiuolo G, Barra M, Preziosi V, Cassinese A, Rotoli B, Guido S. Microfluidics analysis of red blood cell membrane viscoelasticity. Lab Chip 2011;11:449–54.

[3] Bao G, Suresh S. Cell and molecular mechanics of biological materials. Nat Mater 2003;2:715–25.
[4] Park YK, Best CA, Badizadegan K, Dasari RR, Feld MS, Kuriabova T, Henle ML, Levine AJ, Popescu G. Measurement of red blood cell mechanics during morphological changes. Proc Natl Acad Sci USA 2010;107:6731–6.
[5] Dharmadhikari JA, Roy S, Dharmadhikari AK, Sharma S, Mathur D. Torque-generating malaria-infected red blood cells in an optical trap. Opt Express 2004;12:1179–84.
[6] Maier AG, Cooke BM, Cowman AF, Tilley L. Malaria parasite proteins that remodel the host erythrocyte. Nat Rev Microbiol 2009;7:341–54.
[7] Mohandas N, Gallagher PG. Red cell membrane: past, present, and future. Blood 2008;112:3939–48.
[8] Habaza M, Gilboa B, Roichman Y, Shaked NT. Tomographic phase microscopy with 180° rotation of live cells in suspension by holographic optical tweezers. Opt Lett 2015;40:1881–4.
[9] Dharmadhikari JA, Roy S, Dharmadhikari AK, Sharma S, Mathur D. Naturally occurring, optically driven, cellular rotor. Appl Phys Lett 2004;85:6048–50.
[10] Locovei S, Bao L, Dahl G. Pannexin 1 in erythrocytes: function without a gap. Proc Natl Acad Sci USA 2006;103:7655–9.
[11] Price AK, Fischer DJ, Martin RS, Spence DM. Deformation-induced release of ATP from erythrocytes in a poly(dimethylsiloxane)-based microchip with channels that mimic resistance vessels. Anal Chem 2004;76:4849–55.
[12] Forsyth AM, Wan JD, Owrutsky PD, Abkarian M, Stone HA. Multiscale approach to link red blood cell dynamics, shear viscosity, and ATP release. Proc Natl Acad Sci USA 2011;108:10986–91.
[13] Saux BL, Chalmond B, Yu Y, Trouvé A, Renaud O, Shorte SL. Isotropic high-resolution three-dimensional confocal micro-rotation imaging for non-adherent living cells. J Microsc 2009;233:404–16.
[14] Kolb T, Albert S, Haug M, Whyte G. Dynamically reconfigurable fibre optical spanner. Lab Chip 2014;14:1186–90.
[15] Mohanty K, Mohanty S, Monajembashi S, Greulich KO. Orientation of erythrocytes in optical trap revealed by confocal fluorescence microscopy. J Biomed Opt 2007;12:060506.
[16] Li X, Chen WQ, Liu GY, Lu W, Fu JP. Continuous-flow microfluidic blood cell sorting for unprocessed whole blood using surface-micromachined microfiltration membranes. Lab Chip 2014;14:2565–75.
[17] Shin S, Hou, JX, Suh JS, Singh M. Validation and application of a microfluidic ektacytometer (RheoScan-D) in measuring erythrocyte deformability. Clin Hemorheol Microcirc 2007;37:319–28.
[18] Guo Q, Parka S, Ma HS. Microfluidic micropipette aspiration for measuring the deformability of single cells. Lab Chip 2012;12:2687–95.
[19] Engelhardt H, Gaub H, Sackmann E. Viscoelastic properties of erythrocyte membranes in high-frequency electric fields. Nature 1984;307:378–80.
[20] Cross SE, Jin Y-S, Rao JY, Gimzewski JK. Nanomechanical analysis of cells from cancer patients. Nat Nanotechnol 2007;2:780–3.
[21] Xin H, Li Y, Liu X, Li B. *Escherichia coli*-based biophotonic waveguides. Nano Lett 2013;13:3408–13.
[22] Liu X, Huang J, Zhang Y, Li B. Optical regulation of cell chain. Sci Rep 2015;5:11578.
[23] Fazal FM, Block SM. Optical tweezers study life under tension. Nat Photonics 2011;5:318–21.
[24] Gross SP. Application of optical traps in vivo. Methods Enzymol 2003;361:162–74.
[25] Guck J, Ananthakrishnan R, Mahmood H, Moon TJ, Cunningham CC, Käs J. The optical stretcher: a novel laser tool to micromanipulate cells. Biophys J 2001;81:767–84.
[26] Kuś A, Dudek M, Kemper B, Kujawińska M, Vollmer A. Tomographic phase microscopy of living three-dimensional cell cultures. J Biomed Opt 2014;19:046009.
[27] Kreysing MK, Kießling T, Fritsch A, Dietrich C, Guck JR, Käs JA. The optical cell rotator. Opt Express 2008;16:16984–92.
[28] Rancourt-Grenier S, Wei MT, Bai JJ, Chiou A, Bareil PP, Duval PL, Sheng Y. Dynamic deformation of red blood cell in dual-trap optical tweezers. Opt Express 2010;18:10462–72.

Supplemental Material: The online version of this article (DOI: 10.1515/nanoph-2016-0115) offers supplementary material, available to authorized users.